



Moving-Mesh Methods for One-Dimensional Hyperbolic Problems Using CLAWPACK

R. FAZIO

Department of Mathematics, University of Messina, 98165 Messina, Italy
rfazio@dipmat.unime.it

R. J. LEVEQUE

Department of Applied Mathematics and Department of Mathematics,
University of Washington, Box 352420, Seattle, WA 98195-2420, U.S.A.
rjl@amath.washington.edu

Abstract—We develop a one-dimensional moving-mesh method for hyperbolic systems of conservation laws. This method is based on the high-resolution finite-volume “wave-propagation method”, implemented in the CLAWPACK software package. A modified system of conservation laws is solved on a fixed, uniform computational grid, with a grid mapping function computed simultaneously in such a way that in physical space certain features are tracked by cell interfaces. The method is tested on a shock-tube problem with multiple reflections where the contact discontinuity is tracked, and also on two multifluid problems where the interface between two distinct gases is tracked. One is a standard test problem and the other also involves a moving piston whose motion is also tracked by the moving mesh. © 2003 Elsevier Science Ltd. All rights reserved.

Keywords—Moving-mesh methods, Finite-volume methods, Hyperbolic conservation laws, Interface problems.

1. INTRODUCTION

We study high-resolution finite-volume methods for the one-dimensional conservation law

$$q_t + f(q)_x = \psi(x, q) \quad (1)$$

on a moving grid, where the interface x_i^n between grid cells varies with time t_n . Figure 1 shows a typical moving grid over one time step. We show how the wave-propagation algorithms developed in [1] and implemented in the CLAWPACK software [2] can be modified to handle moving grids, and consider applications to gas dynamics in a tube with moving-piston boundary conditions and also a moving interface between two gases.

With a finite volume method, our approximation consists of cell averages

$$Q_i^n \approx \frac{1}{\Delta x_i^n} \int_{x_i^n}^{x_{i+1}^n} q(x, t_n) dx,$$

The first author would like to express his thanks for the support by a NATO-CNR grant (No. 217.28/01) and the kind hospitality of the Department of Applied Mathematics of the Washington University. The second author has been supported in part by DOE Grant DE-FG03-96ER25292 and NSF Grants DMS-9505021 and DMS-9626645.

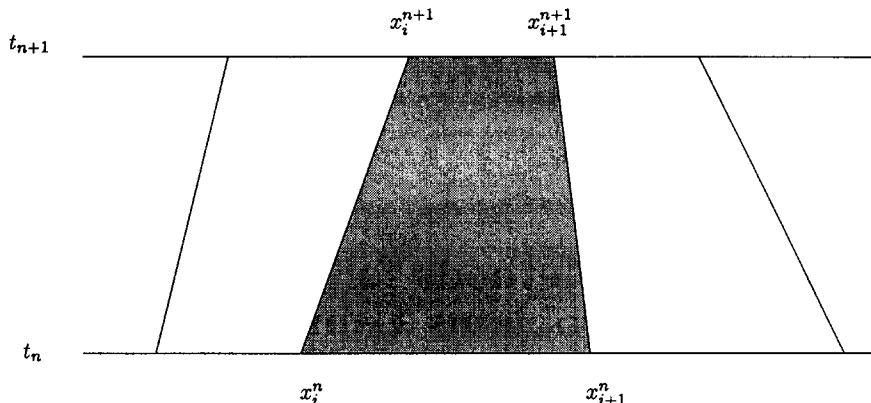


Figure 1. Grid points in the moving-mesh method. The conservation law is integrated over a typical grid cell in space-time, shown shaded. The cell interfaces move with velocities \dot{x}_i^n and \dot{x}_{i+1}^n , respectively.

where $\Delta x_i^n = x_{i+1}^n - x_i^n$ and the grid is illustrated in Figure 1. We assume the motion of x_i has constant speed

$$\dot{x}_i^n = \frac{x_i^{n+1} - x_i^n}{\Delta t}$$

over each time step $[t_n, t_{n+1}]$. By integrating the conservation law over the shaded trapezoid in Figure 1, we obtain an expression for the cell average Q_i^{n+1} at time t_{n+1} in terms of Q_i^n and the fluxes across the rays $x = x_i^n + \dot{x}_i^n(t - t_n)$ and $x = x_{i+1}^n + \dot{x}_{i+1}^n(t - t_n)$ bounding the trapezoid on the left and right. A numerical method is obtained by approximating the fluxes on the basis of nearby cell averages.

Harten and Hyman [3] show how to extend Godunov’s method and Roe’s method (based on approximate Riemann solvers) to this context. They also proposed a method for moving the grid (i.e., choosing the speed \dot{x}_i^n in each step) to improve the resolution of shocks and contact discontinuities in gas dynamics problems. The Godunov and Roe methods are only first-order accurate. Here we show how the high-resolution algorithms implemented in CLAWPACK can be easily extended to the moving grid. In one space dimension, this algorithm is very similar to other flux-limiter or slope-limiter methods that have been proposed in the literature. The extension to moving grids is made with a simple modification of the Riemann solver and appropriate use of the “capacity function” discussed in [1].

This algorithm could then be combined with the moving-mesh algorithm of Harten and Hyman. Rather than pursuing this, we instead study three specific problems where the mesh motion is chosen to explicitly track moving interfaces and/or boundaries. In particular, we study a gas in a tube bounded by a solid wall at $x = 0$ and a moving piston at $x = L(t)$. We could solve this classical piston problem using N grid cells in $[0, L(t)]$ with cell interfaces $x_i^n = (i - 1)\Delta x_i^n$, where $\Delta x_i^n = L(t_n)/N$. To make the problem more interesting, we also assume the tube contains two different gases separated by a contact discontinuity at some point $I(t) < L(t)$. In this case, we can choose the grid motion so that the gas interface is always at a cell interface, allowing sharp resolution and simple solution of the two-fluid Riemann problem at the interface.

By including a source term in (1), we can also solve spherically symmetric problems in three space dimensions, where x now represents distance from the origin. In particular, the two-fluid case could potentially be extended to model a spherically-symmetric bubble. A gas-filled bubble in liquid might be modeled by using, for example, the Tait equation of state in the outer fluid (for $x > I(t)$). The study of gas bubbles is of interest in a variety of applications, including sonoluminescence, in which sound waves in the liquid cause such violent contraction of small gas bubbles that light is emitted via some mechanism that is not yet understood. Focusing shock waves within the bubble may be of importance and there is interest in modeling such dynamics [4].

Another possible application is to nonlinear acoustic or elastic waves in a heterogeneous solid, where the grid motion could follow deformations of an elastic body to keep the material properties of each grid cell fixed. CLAWPACK has been shown to work well on linear [5] or weakly nonlinear [6] problems with rapidly varying material properties, where the variation of coefficients with x is held fixed independent of the solution. The moving-mesh method developed here should allow these studies to be carried further to fully nonlinear problems where the movement of the material is significant.

In this paper, we concentrate on describing the moving mesh and interface tracking algorithm, which may be of interest in other applications as well, and only consider the case of a single gamma-law gas or two ideal gases with different values of γ . Several examples are presented in Section 6.

Many other moving-mesh methods for hyperbolic problems have been proposed in the literature. Some recent references include [7–12].

The approach proposed here has the advantage that it is easily implemented using the CLAWPACK software package, not only for the gas dynamics problems used here as examples, but for a wide variety of other problems where CLAWPACK applies. A sample code is available from the CLAWPACK web page [2] which can be used as a template for other applications. See <http://www.amath.washington.edu/~rjl/clawpack/movingmesh>.

2. THE MODIFIED ALGORITHMS

Our description of the algorithms follows the notation of [1]. Let $0 \leq \xi \leq 1$ be the “computational domain” in which we have a fixed uniform grid with $\xi_i = (i - 1)\Delta\xi$ for $i = 1, 2, \dots, N + 1$, with $\Delta\xi = 1/N$. We also have a grid mapping $X(\xi, t)$ with the property that

$$x_i^n = X(\xi_i, t_n).$$

Computationally, we will assume that the time derivative $X_t(\xi_i, t)$ is constant over $t_n < t < t_{n+1}$, and this is what we call \dot{x}_i^n , but before discussing the computational algorithm, it is illuminating to consider the transformation of the differential equation (1) to an equation in (ξ, t) using a smooth mapping function $X(\xi, t)$.

Let $\tilde{q}(\xi, t) \equiv q(X(\xi, t), t)$ and $\tilde{\psi}(\xi, \tilde{q}) = \psi(X(\xi, t), \tilde{q})$. Then we compute

$$\begin{aligned} f(\tilde{q})_\xi = f(q)_x X_\xi &\implies f(q)_x = \frac{f(\tilde{q})_\xi}{X_\xi}, \\ \tilde{q}_t = q_t + X_t(\xi, t)q_x = q_t + \frac{X_t \tilde{q}_\xi}{X_\xi} &\implies q_t = \tilde{q}_t - \frac{X_t \tilde{q}_\xi}{X_\xi}. \end{aligned}$$

Inserting these in equation (1) and multiplying by X_ξ gives

$$X_\xi \tilde{q}_t + f(\tilde{q})_\xi - X_t \tilde{q}_\xi = X_\xi \tilde{\psi}. \quad (2)$$

We can put the left-hand side in conservation form by noting that

$$\begin{aligned} X_\xi \tilde{q}_t &= (X_\xi \tilde{q})_t - X_{\xi t} \tilde{q}, \\ X_t \tilde{q}_\xi &= (X_t \tilde{q})_\xi - X_{t\xi} \tilde{q}, \end{aligned}$$

and so (2) becomes

$$(X_\xi \tilde{q})_t + [f(\tilde{q}) - X_t \tilde{q}]_\xi = X_\xi \tilde{\psi}. \quad (3)$$

We could now proceed by discretizing either (2) or (3) over the uniform computational grid in ξ . However, to insure conservation, we will instead derive the method based on integration over the trapezoid in Figure 1 and then see that this gives a consistent approximation to these equations.

We first consider the homogeneous case $\psi \equiv 0$ and the use of Godunov’s method with the exact Riemann solver. We approximate q by a piecewise constant function at time t_n and can then compute the exact update based on the values Q_i^* which are defined to be the state obtained in the Riemann problem between Q_{i-1}^n and Q_i^n along the ray $(x - x_i^n)/(t - t_n) = \dot{x}_i^n$ between the grid cells. Integrating the conservation law over the trapezoid as in [3] gives the following expression:

$$\Delta x_i^{n+1} Q_i^{n+1} = \Delta x_i^n Q_i^n - \Delta t [(f(Q_{i+1}^*) - \dot{x}_{i+1}^n Q_{i+1}^*) - (f(Q_i^*) - \dot{x}_i^n Q_i^*)]. \tag{4}$$

Define $\kappa_i^n = \Delta x_i^n / \Delta \xi$. Then replacing Δx_i^n by $\kappa_i^n \Delta \xi$ and dividing by $\Delta \xi$ in (4) gives

$$\kappa_i^{n+1} Q_i^{n+1} = \kappa_i^n Q_i^n - \frac{\Delta t}{\Delta \xi} [(f(Q_{i+1}^*) - \dot{x}_{i+1}^n Q_{i+1}^*) - (f(Q_i^*) - \dot{x}_i^n Q_i^*)]. \tag{5}$$

Note that this gives a consistent approximation to (3) (when $\psi = 0$) since

$$\kappa_i^n \approx X_\xi(\xi_i, t_n) \quad \text{and} \quad \dot{x}_i^n \approx X_t(\xi_i, t_n).$$

The description of wave propagation algorithms in [1] includes a discussion of how to handle general capacity functions $\kappa(\xi)$ in the equation $\kappa(\xi)q_t + f(q)_\xi = 0$, in the case when κ is independent of time. The general idea of κ is that $\kappa_i \Delta \xi$ represents the “capacity” of the i^{th} cell, either due to variable grid spacing as here, or to other physical effects such as variable porosity in a porous media problem.

Now κ varies with t as well. As discussed in [1], we would like to write the algorithm in a form that achieves two goals.

1. $\sum \kappa_i^n Q_i^n$ should be conserved with n .
2. Constant states q should be preserved, even when κq is varying, since in this case $q_x \equiv 0$ implies $f(q)_x \equiv 0$.

When κ_i^n is independent of n , this can be achieved by dividing (5) by κ_i and incorporating κ_i properly in the correction terms for the high-resolution method discussed below. When the grid is moving and κ_i^n varies with n , we must first rewrite (5) using the observation

$$\kappa_i^n Q_i^n = \kappa_i^{n+1} Q_i^n - \frac{\Delta t}{\Delta \xi} (\dot{x}_{i+1}^n - \dot{x}_i^n) Q_i^n,$$

which follows from the fact that $x_i^{n+1} = x_i^n + \Delta t \dot{x}_i^n$. Using this in (5) and rearranging gives

$$\kappa_i^{n+1} Q_i^{n+1} = \kappa_i^{n+1} Q_i^n - \frac{\Delta t}{\Delta \xi} [(f(Q_{i+1}^*) - \dot{x}_{i+1}^n (Q_{i+1}^* - Q_i^n)) - (f(Q_i^*) - \dot{x}_i^n (Q_i^* - Q_i^n))]. \tag{6}$$

Note that this can be viewed as a discretization of equation (2) when $\psi = 0$.

When a source term $\psi(x)$ is present, we must include an approximation to the integral over the trapezoid, with appropriate weighting,

$$\kappa(x, t) \int_{t_n}^{t_{n+1}} \left[\frac{1}{x_{i+1}(t) - x_i(t)} \int_{x_i(t)}^{x_{i+1}(t)} \psi(x, q) dx \right] dt$$

in update (6). This can be approximated to first order by $\kappa_i^{n+1} \Delta t \psi(Q_i^n)$, or a fractional step method such as the Strang splitting implemented in CLAWPACK could be used to incorporate this term.

Here, we are assuming that κ is nonzero everywhere. This ensures a nonsingular grid mapping $X(\xi, t)$, and hence, a one-to-one and onto mapping between the computational and the physical domain. A similar grid mapping, but singular at the initial time, was used in [13] to study a shock propagation in a thin elastic rod.

3. IMPLEMENTATION

The CLAWPACK software can be applied directly to implement (6) if we simply modify the code to use κ_i^{n+1} as the capacity function in step n and modify the standard Riemann solver to return modified flux differences that incorporate the grid motion.

The standard Riemann solver (for the case $\dot{x}_i^n = 0$) returns flux differences (see [1])

$$\begin{aligned}\mathcal{A}^- \Delta q_i &= f(Q_i^*) - f(Q_{i-1}), \\ \mathcal{A}^+ \Delta q_i &= f(Q_i) - f(Q_i^*),\end{aligned}\tag{7}$$

where Q_i^* is the solution along $(x - x_i^n)/(t - t_n) = 0$ in this case. The update formula for Godunov's method is

$$Q_i^{n+1} = Q_i^n - \frac{\Delta t}{\kappa_i \Delta \xi} (\mathcal{A}^+ \Delta q_i + \mathcal{A}^- \Delta q_{i+1}).\tag{8}$$

When $\dot{x}_i^n \neq 0$, we simply modify this routine so that Q_i^* is the solution along the ray $(x - x_i^n)/(t - t_n) = \dot{x}_i^n$ and so that we return

$$\begin{aligned}\mathcal{A}^- \Delta q_i &= f(Q_i^*) - f(Q_{i-1}) - \dot{x}_i^n (Q_i^* - Q_{i-1}), \\ \mathcal{A}^+ \Delta q_i &= f(Q_i) - f(Q_i^*) - \dot{x}_i^n (Q_i - Q_i^*).\end{aligned}\tag{9}$$

The update formula (8) is unchanged except that κ_i now varies in time and we use κ_i^{n+1} .

If the Roe approximate Riemann solver is used, then the solution to the Riemann problem is approximated by solving some linear system $q_t + A_i q_x = 0$ with $A \in \mathbb{R}^{m \times m}$ for a system of m equations. This yields a decomposition of $\Delta Q_i = Q_i - Q_{i-1}$ into waves \mathcal{W}_i^p and speeds λ_i^p (for $p = 1, 2, \dots, m$) so that

$$Q_i - Q_{i-1} = \sum_p \mathcal{W}_i^p \quad \text{and} \quad f(Q_i) - f(Q_{i-1}) = \sum_p \lambda_i^p \mathcal{W}_i^p.$$

For the case $\dot{x}_i^n = 0$, the flux differences are then

$$\begin{aligned}\mathcal{A}^- \Delta q_i &= \sum_p (\lambda_i^p)^- \mathcal{W}_i^p, \\ \mathcal{A}^+ \Delta q_i &= \sum_p (\lambda_i^p)^+ \mathcal{W}_i^p,\end{aligned}\tag{10}$$

where $\lambda^- = \min(\lambda, 0)$ and $\lambda^+ = \max(\lambda, 0)$. These are very easily generalized to the case $\dot{x}_i^n \neq 0$. The waves and speeds are calculated as before and we then set

$$\begin{aligned}\mathcal{A}^- \Delta q_i &= \sum_p (\lambda_i^p - \dot{x}_i^n)^- \mathcal{W}_i^p, \\ \mathcal{A}^+ \Delta q_i &= \sum_p (\lambda_i^p - \dot{x}_i^n)^+ \mathcal{W}_i^p.\end{aligned}\tag{11}$$

If an entropy fix is included in the definition of $\mathcal{A}^- \Delta q$ and $\mathcal{A}^+ \Delta q$, then we must be sure to use the shifted wave speeds also in this calculation, as discussed in [3].

4. HIGH-RESOLUTION METHODS

High-resolution methods are implemented in CLAWPACK by adding an additional term to the update, obtaining

$$Q_i^{n+1} = Q_i^n - \frac{\Delta t}{\kappa_i^{n+1} \Delta \xi} (\mathcal{A}^+ \Delta q_i + \mathcal{A}^- \Delta q_{i+1}) - \frac{\Delta t}{\kappa_i^{n+1} \Delta \xi} (\tilde{F}_{i+1}^n - \tilde{F}_i^n),$$

where

$$\tilde{F}_i^n = \frac{1}{2} \sum_{p=1}^m |\tilde{\lambda}_i^p| \left(1 - \frac{\Delta t}{\kappa_{i-1/2}^{n+1} \Delta \xi} |\tilde{\lambda}_i^p| \right) \tilde{\mathcal{W}}_i^p.$$

Here $\tilde{\mathcal{W}}_i^p$ is a limited version of \mathcal{W}_i^p (see [1]) and

$$\tilde{\lambda}_i^p = \lambda_i^p - \dot{x}_i^n$$

is again the shifted wave speed if the grid is moving. The average value $\kappa_{i-1/2} \equiv (1/2)(\kappa_{i-1} + \kappa_i)$ is used since $\kappa_{i-1/2} \Delta \xi$ models the distance between cell centers. This should more properly be evaluated at time t_n rather than t_{n+1} , but if the mesh is varying smoothly this affects only higher-order terms and the above approach arises naturally since we use κ_i^{n+1} as the capacity function in the n^{th} step.

5. SHOCK TUBE PROBLEMS

In Example 3 of Section 6, we consider a piston moving into a tube filled with two different gases separated by an interface. The moving-mesh method is used to maintain a fixed number of grid cells in the tube of varying length, and also to avoid mixing of the two gases by tracking the contact surface with a grid line.

First, however, we consider a simpler shock tube problem with a single gas in a fixed length tube, with the mesh chosen to follow the contact discontinuity. This is a useful test problem since it leads to a highly distorted mesh but in a situation where a uniform mesh calculation can also be performed for comparison. We will see that the wave-propagation method performs well on the moving mesh, even when there is a large jump in mesh spacing across the contact discontinuity. Moreover, in Example 2, we consider two standard test problems for multifluid methods. In both cases, the reported numerical results demonstrate that the proposed moving-mesh method can be applied also to the interaction of strong shock waves with contact discontinuities.

In all of these test problems, we use the Euler equations of gas dynamics,

$$q_t + f(q)_x = 0,$$

where

$$q = \begin{bmatrix} \rho \\ \rho u \\ E \end{bmatrix} \quad \text{and} \quad f(q) = \begin{bmatrix} \rho u \\ \rho u^2 + p \\ u(E + p) \end{bmatrix},$$

with the ideal gas equation of state

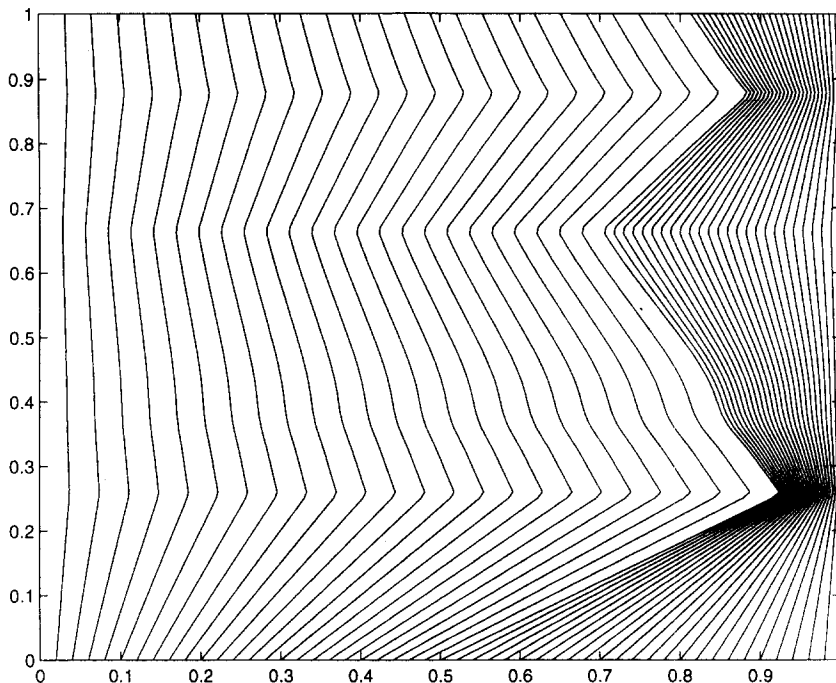
$$p = (\gamma - 1) \left(E - \frac{1}{2} \rho u^2 \right).$$

These equations are solved in the domains $0 \leq x \leq I(t)$ and $I(t) \leq x \leq L(t)$, where $I(t)$ represents the location of a contact discontinuity between two initially separated gases and $L(t)$ is the location of the right boundary. In Examples 1 and 2, $L(t) \equiv 1$ while in Example 3 $L(t)$ tracks the motion of the moving piston. In Example 1, the two gases are the same and $\gamma = 1.4$ everywhere. In Example 2, two different gases are involved, namely, air/helium in Case 1 and air/R22 in Case 2. In Example 3, there are two different gases with $\gamma = 1.4$ for $0 \leq x < I(t)$ while $\gamma = 2.8$ for $I(t) < x \leq L(t)$.

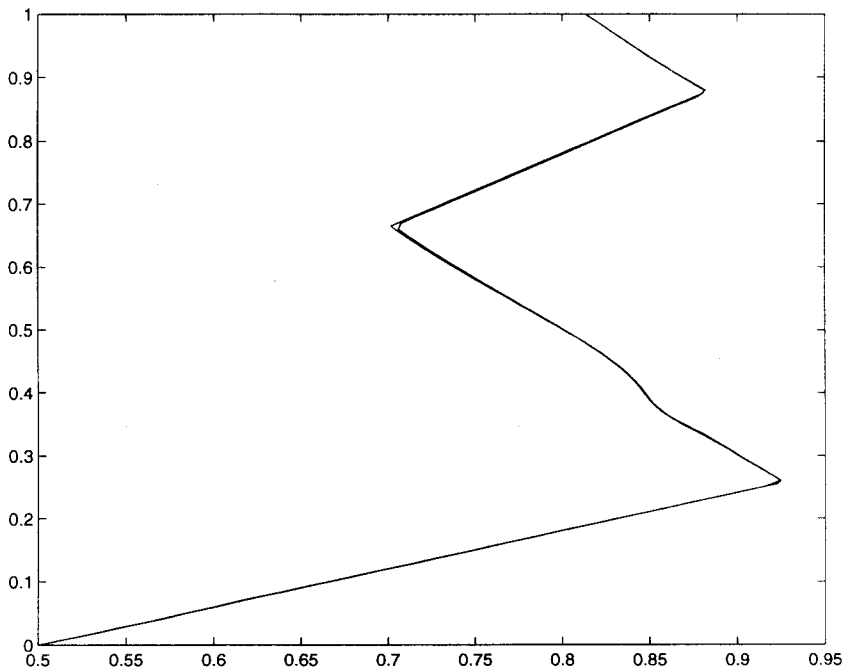
In all cases, we solve on a grid in computational space $0 \leq \xi \leq 1$ with uniform spacing $\Delta \xi$. The grid mapping to physical space is given by

$$X(\xi, t) = \begin{cases} 2\xi I(t), & \text{if } 0 \leq \xi \leq 0.5, \\ I(t) + 2(\xi - 0.5)(L(t) - I(t)), & \text{if } 0.5 \leq \xi \leq 1. \end{cases} \tag{12}$$

Note that the midpoint $\xi = 0.5$ of the computational domain is always mapped to the contact discontinuity $I(t)$. This mapping will not generally be smooth at $\xi = 0.5$ and there may be quite a large jump in the physical mesh spacing Δx at the contact discontinuity if $I(t)$ is far from $L(t)/2$. See Figure 2 for an example.



(a) Motion of grid lines for the moving grid method on Example 1. Every second cell interface from the 100-cell calculation is plotted over time. (Moving-mesh points, $N = 100$.)



(b) Motion of the contact discontinuity $I(t)$ as computed with the moving-mesh method, for both the 100-cell and 2000-cell calculation, plotted together. (Contact location for $N = 100$ and $N = 2000$.)

Figure 2.

It might be preferable to use a nonuniform distribution of grid cells on each side of the contact so that the cell width would vary smoothly rather than being discontinuous across the contact surface. We used (12) in part to demonstrate that the algorithm can deal with such mesh discontinuities.

The mesh movement in each time step is determined by the following procedure: at the beginning of each step, we know $x_i^n = X(\xi_i, t_n)$. We first solve the Riemann problem at $i = N/2$ (assuming N is even), which is at $\xi = 1/2$, corresponding to the contact discontinuity $x = I(t_n)$ in physical space. In solving this Riemann problem, we must take into account the fact that γ may be different on each side of the resulting contact discontinuity, which is the two-wave. The one-wave and three-wave are each in a different gas. This is a simple modification to the standard Riemann solver (see the software). Let \dot{I}^n be the speed of the contact discontinuity resulting from this Riemann problem, i.e., $\dot{I}^n = \lambda_{N/2}^2$ in the standard notation for wave speeds. This approximates $I'(t_n)$ and is the speed used to move the grid. For $i \leq N/2$, the grid then moves according to

$$\dot{x}_i^n = 2\xi_i \dot{I}^n, \quad \text{for } i \leq \frac{N}{2}.$$

When $L(t) \equiv 1$ is fixed, the mesh velocity for $i > N/2$ is also determined directly

$$\dot{x}_i^n = 2(1 - \xi_i) \dot{I}^n, \quad \text{for } i \geq \frac{N}{2}.$$

The case where $L(t)$ varies is discussed in Example 3.

6. NUMERICAL RESULTS

EXAMPLE 1.

Consider a shock tube problem in a fixed tube $0 \leq x \leq 1$ with a single gas (with $\gamma = 1.4$) and initial conditions $\rho \equiv 1$, $u \equiv 0$,

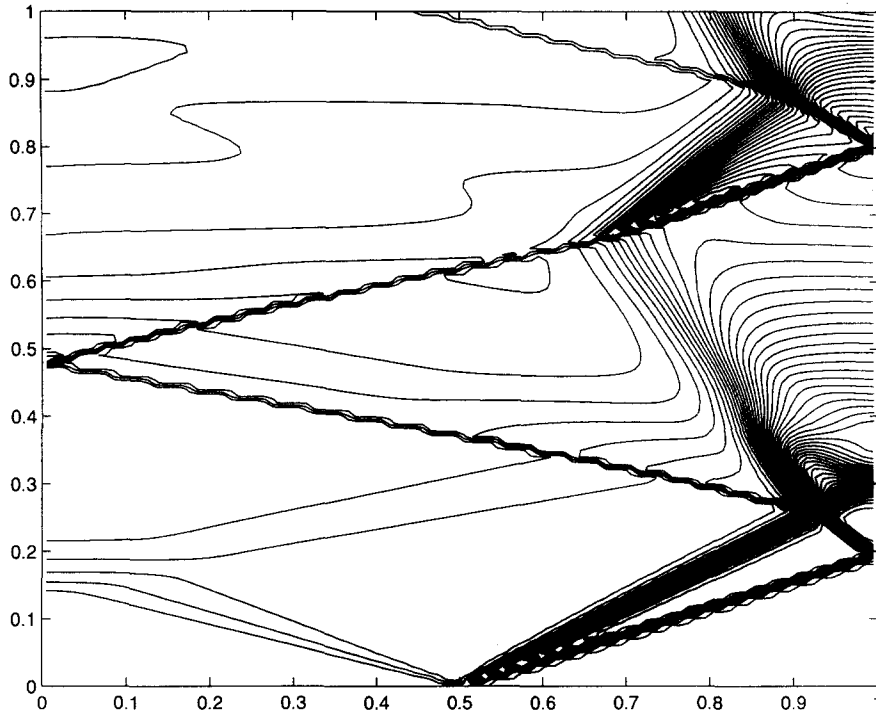
$$p = \begin{cases} 10, & \text{if } x < 0.5, \\ 1, & \text{if } x > 0.5. \end{cases}$$

This gives rise to the wave structure seen in Figures 3 and 4, which show contour plots of the density and velocity in the x - t plane for four different computations. The tube is closed at both ends so that the shock and rarefaction waves reflect. The gas initially occupying $x < 0.5$ and that initially occupying $x > 0.5$ do not mix, but remain separated by a contact discontinuity at some location $I(t)$. The motion of this contact surface is most clearly seen in Figure 2, which shows the motion of the grid lines in a moving-mesh calculation. The mesh was chosen by uniformly stretching or compressing the grid on either side of the contact surface so that there are always an equal number of cells on each side of $I(t)$, using (12). The contact discontinuity then follows a cell interface and is not smeared. On the right of Figure 2, the motion of $I(t)$ for two different resolutions (100 cells and 2000 cells) are plotted together, showing that the coarse grid calculation captures the interface motion very well.

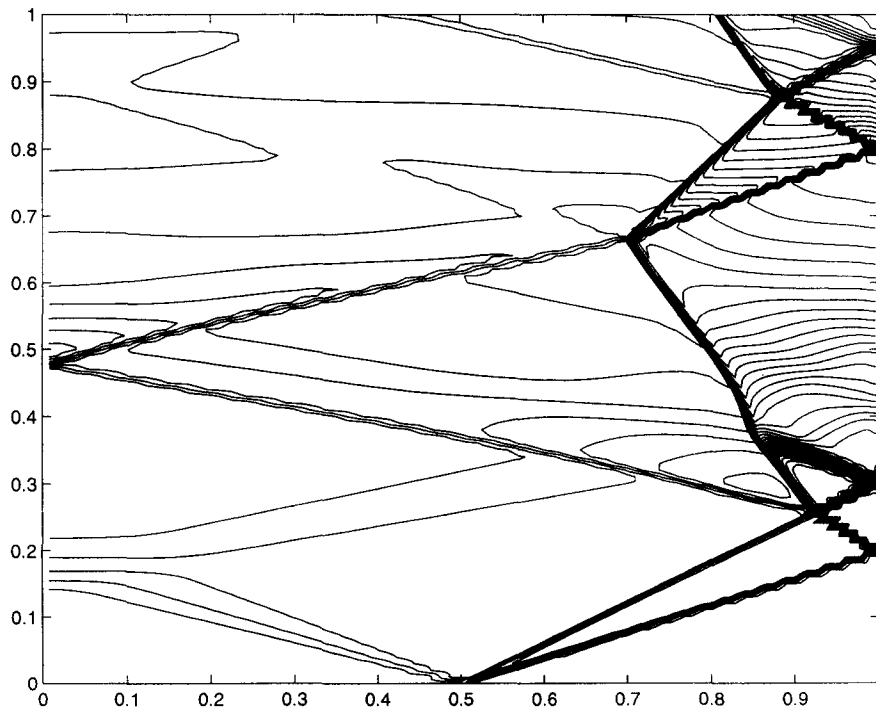
For reference solutions, we performed two different calculations with 2000 mesh cells, one on a uniform mesh and one on the moving mesh. These agreed very well, though the moving-mesh method gave slightly sharper shocks and a sharper contact discontinuity. We then did a comparison of the uniform and moving-mesh methods with only 100 cells in each case. The moving-mesh method performed remarkably better.

Figure 3 shows contour plots of the density from these four calculations. Note that the 100-cell moving-mesh results look nearly as sharp as the 2000-cell uniform mesh results. On the 100-cell uniform mesh, the structure of the contact is nearly completely destroyed when it is hit by the reflected rarefaction wave at $x \approx 0.85$, $t \approx 0.4$.

Figure 4 shows contour plots of the velocity for the same four calculations. The velocity should be continuous across the contact discontinuity. In the moving-mesh plots, the motion of the



(a) Density contours, uniform grid, $N = 100$.



(b) Density contours, moving mesh, $N = 100$.

Figure 3. Contour plots of density in the $x-t$ plane for Example 1, four different computations (x is on the horizontal axis). (a) and (c) are with a uniform grid, (b) and (d) are with the moving-mesh method which tracks the contact discontinuity.

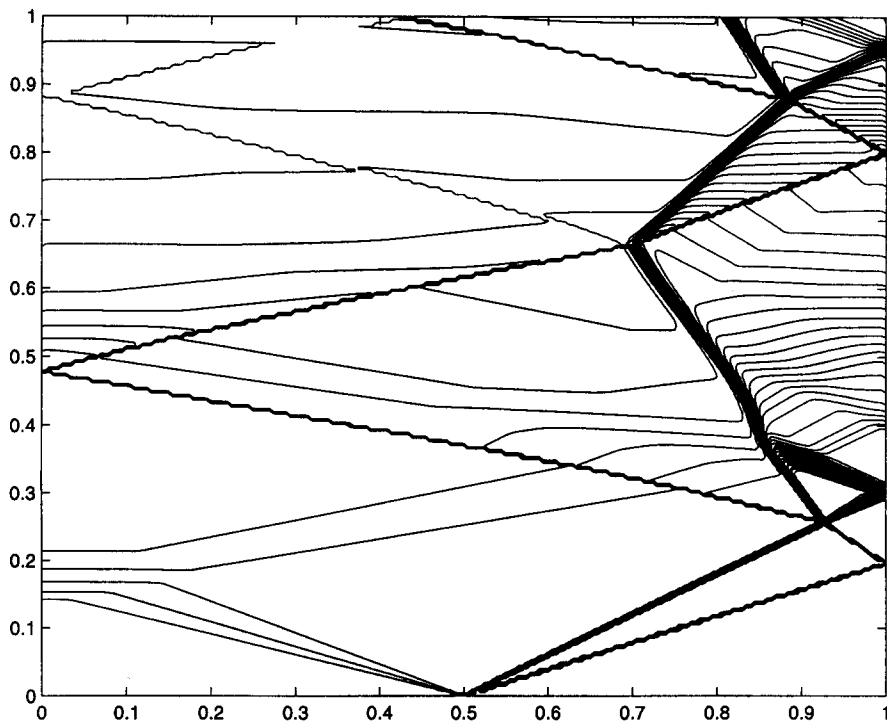
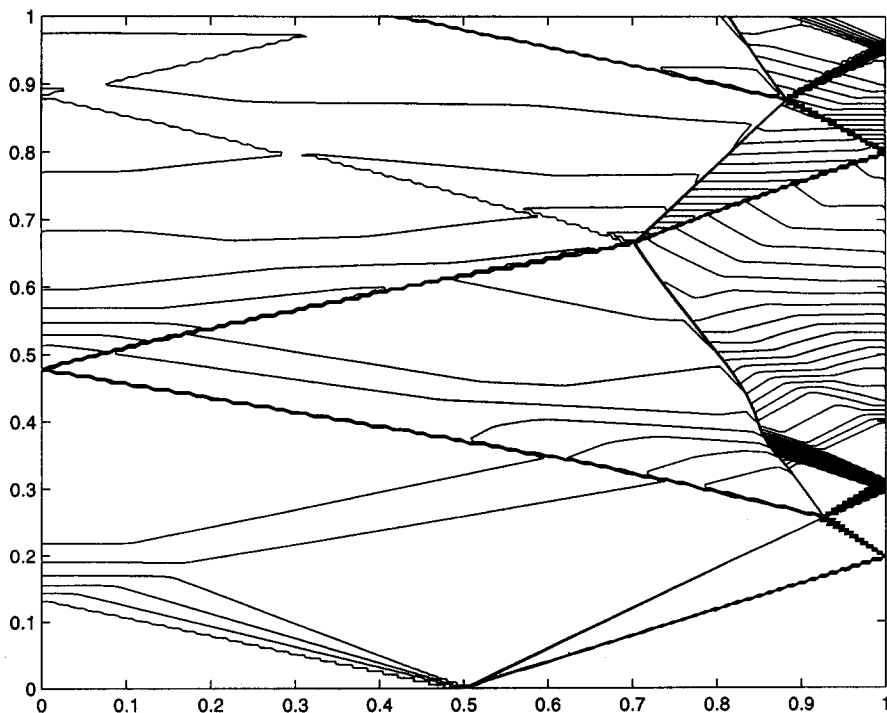
(c) Density contours, uniform grid, $N = 2000$.(d) Density contours, moving mesh, $N = 2000$.

Figure 3. (cont.)

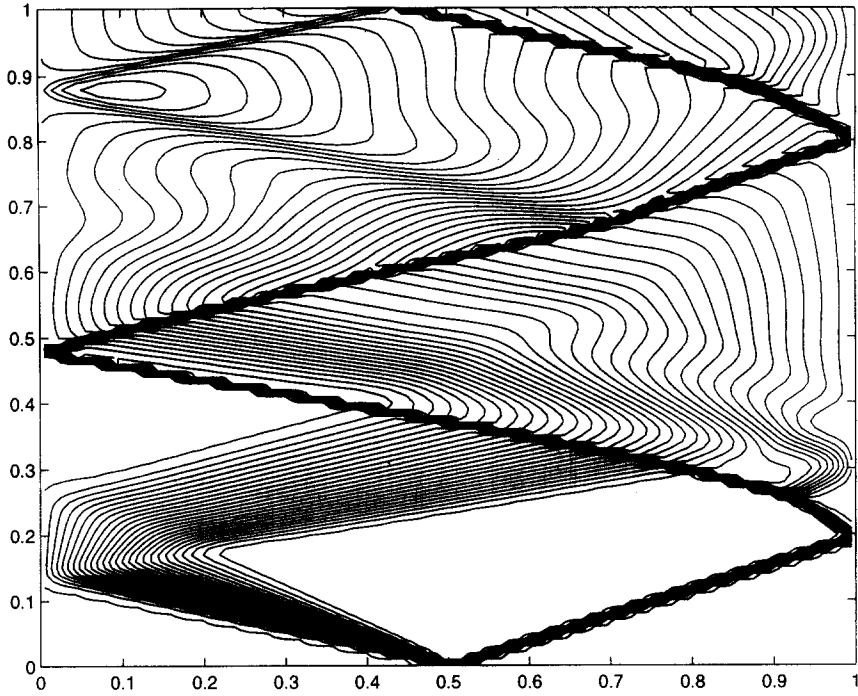
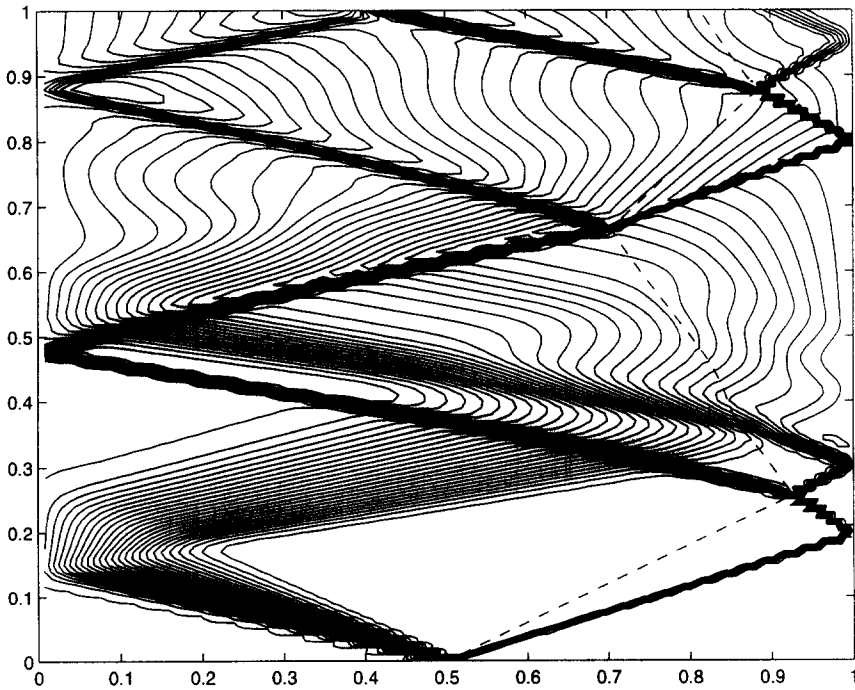
(a) u contours, uniform grid, $N = 100$.(b) u contours, moving mesh, $N = 100$.

Figure 4. Contour plots of velocity in the $x-t$ plane for Example 1, four different computations. (a) and (c) are with a uniform grid, (b) and (d) are with the moving-mesh method which tracks the contact discontinuity. The velocity should be continuous across the contact discontinuity, which is shown in the moving-mesh results as a dashed line.

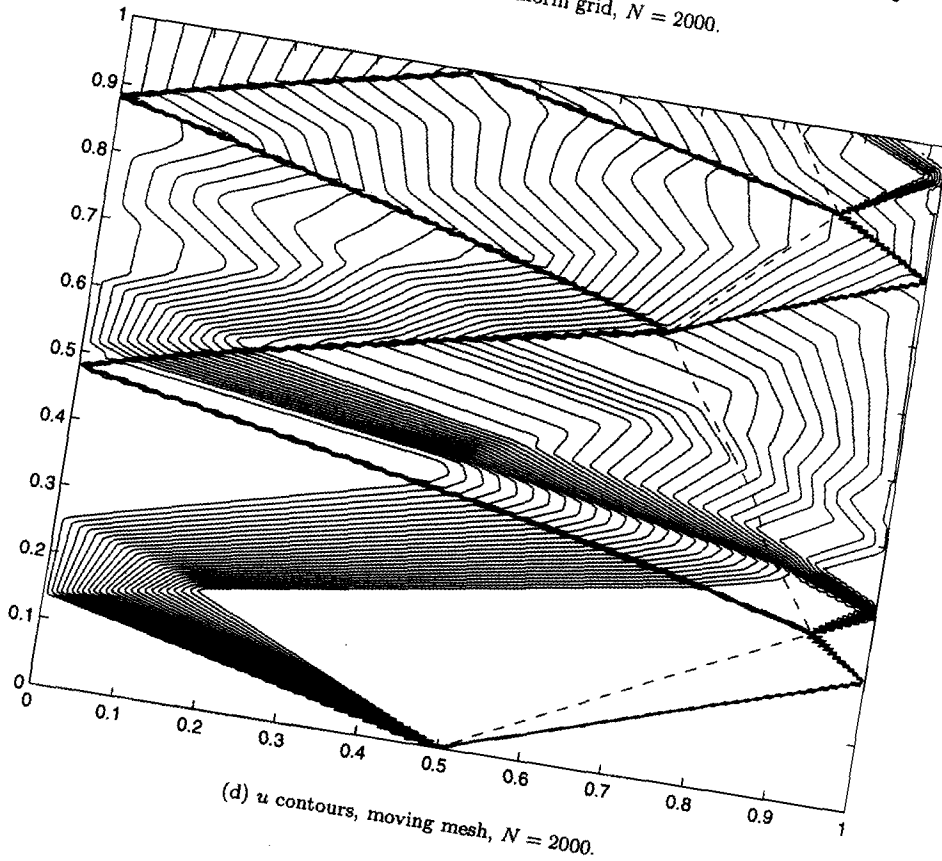
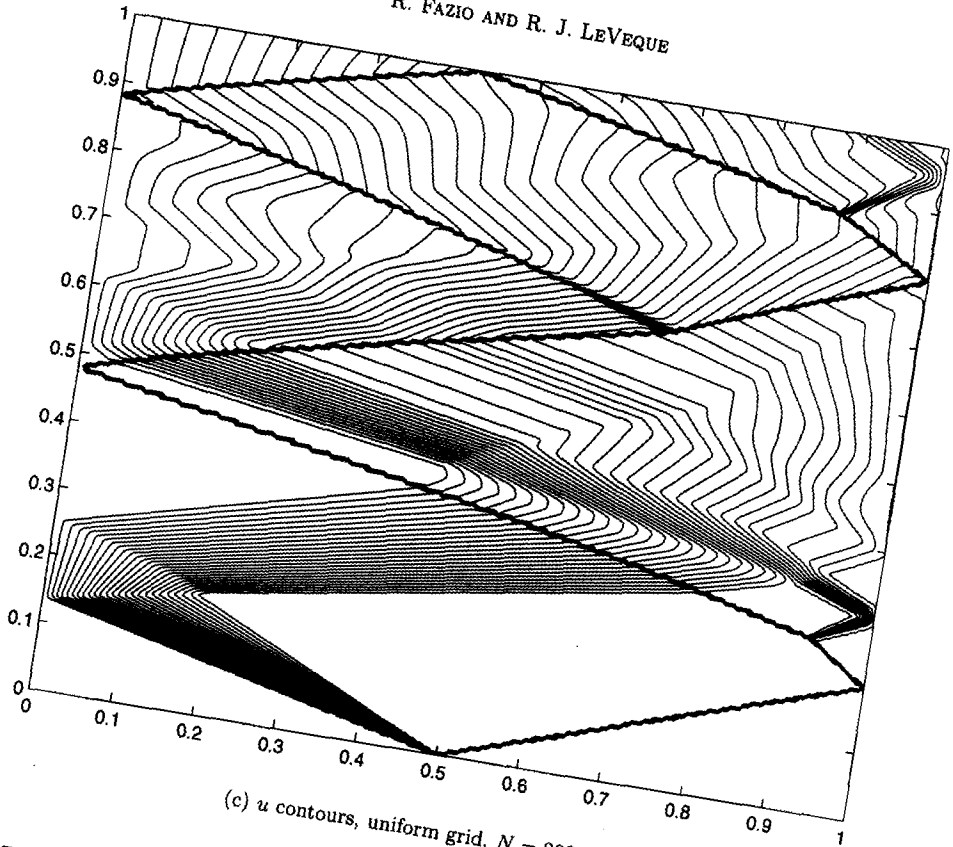


Figure 4. (cont.)

contact is shown by a dashed line for reference. Note that the contours remain smooth across this curve in spite of the discontinuities in mesh width.

The right plot in Figure 2 shows the motion of the contact discontinuity $I(t)$ as computed in the 100-cell and 2000-cell moving-mesh calculations. The two lie on top of one another to plotting accuracy, and over the time period shown agree to within 10^{-3} everywhere.

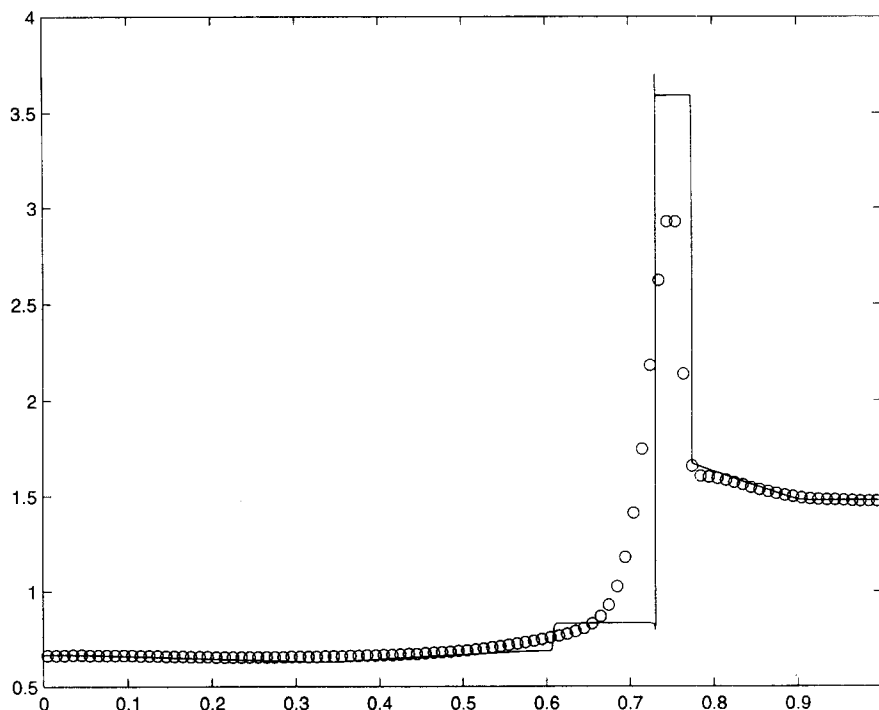
Finally, Figure 5 shows the computed solution (ρ, u, p) at one particular time $t = 0.7$ for the 100-cell uniform mesh (left column) and the 100-cell moving mesh (right column). In each case, the solid line reference solution is from the 2000-cell moving-mesh calculation. Note that on the moving mesh the velocity and pressure are smooth through the contact, which is indicated by the dashed line.

The apparent zig-zag structure of the contour plots are a plotting artifact due to the fact that the solution was output at relatively few times in the t direction.

EXAMPLE 2.

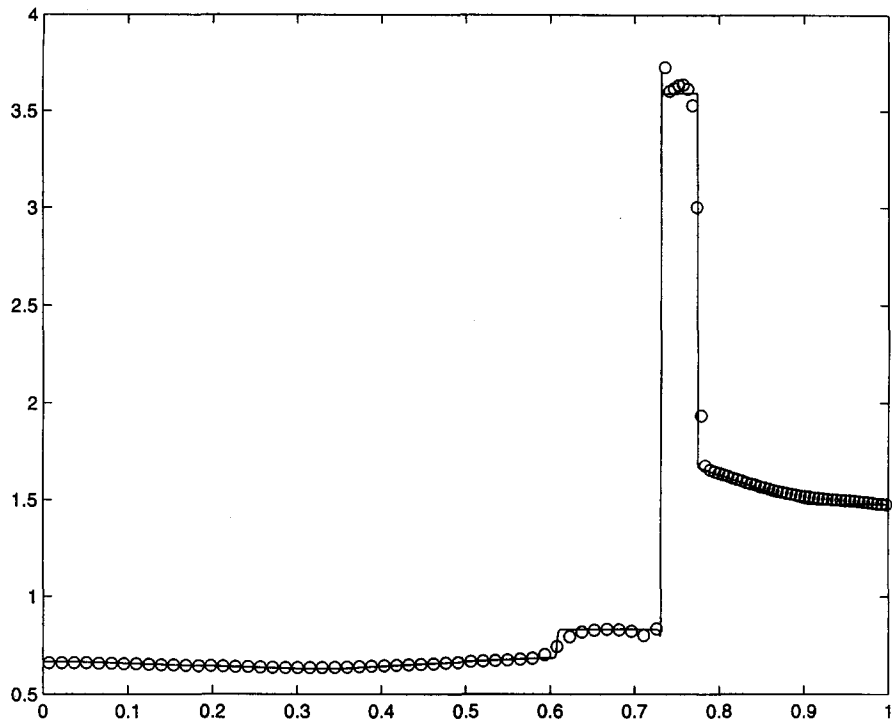
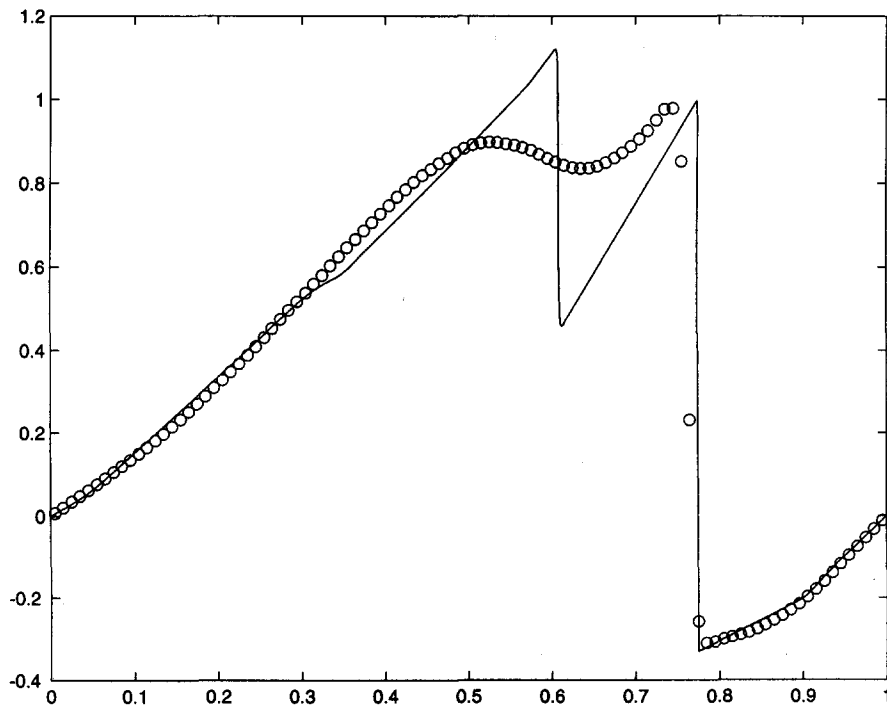
The two tests described in this example were proposed by Karni in order to test her hybrid approach to multifluid flows [14]. Variations of these tests were also used by Jenny, Müller and Thomann [15] and by Fedkiw *et al.* [16].

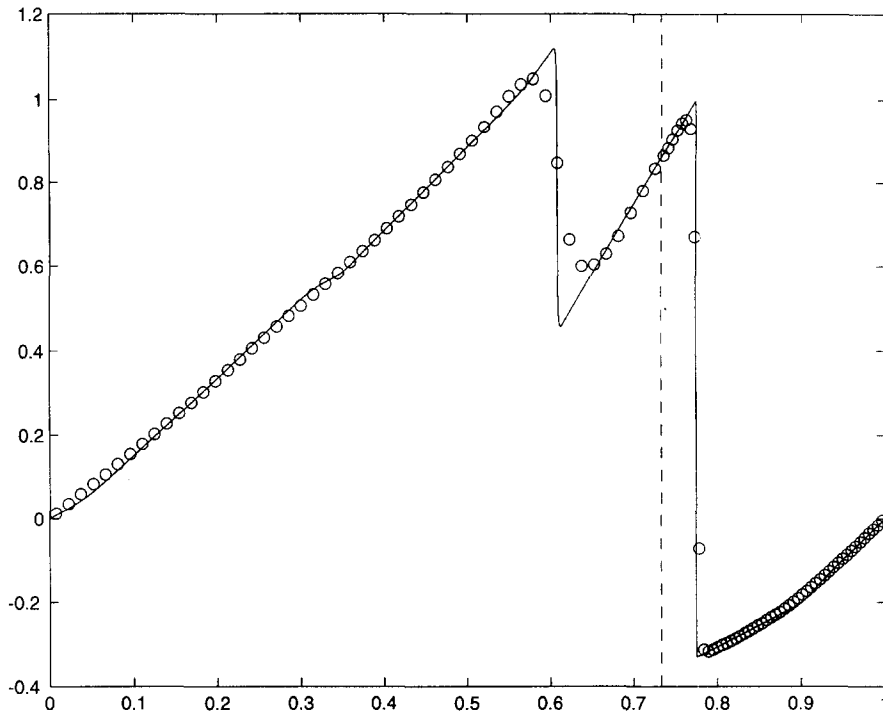
The physical setup for both tests is to consider the interaction of a strong shock (Mach 3.6055) moving from left to right in air with an air/helium (Test D, Case 1 from [14]) or an air/R22 (Test D, Case 2) interface. R22 is the refrigerant commonly known as freon, which is heavier than air. For the numerical results reported below, the initial shock position was set to 0.3 and the initial interface position is at $x = 0.5$. The initial conditions are as follows.



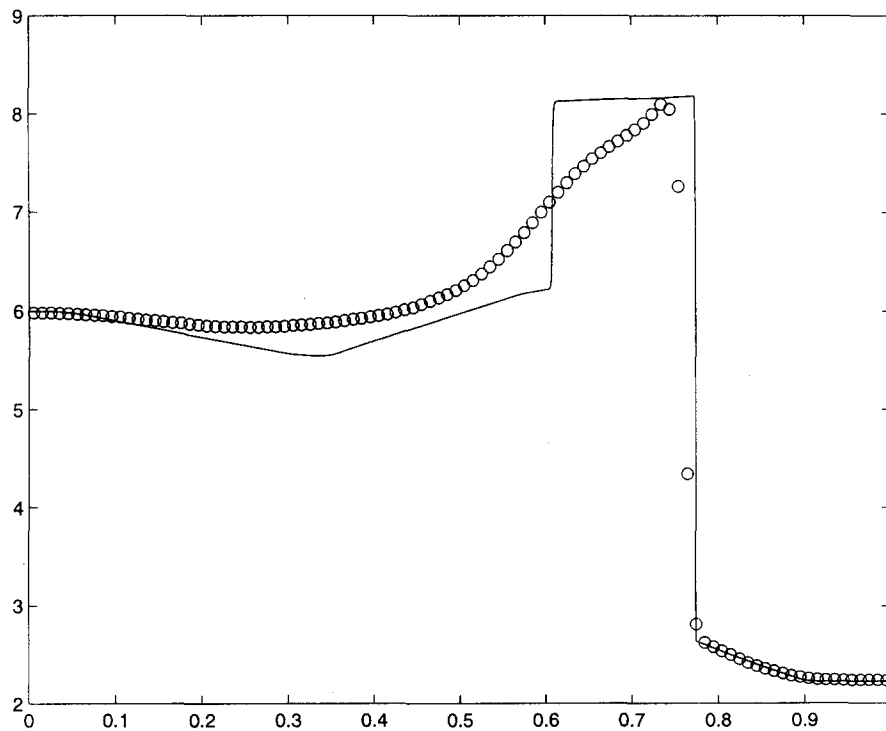
(a) Density at $t = 0.7$, uniform grid, $N = 100$.

Figure 5. The computed solution to Example 1 at one particular time $t = 0.7$ for the 100-cell uniform mesh and the 100-cell moving mesh. In each case, the solid line reference solution is from the 2000-cell moving-mesh calculation. The contact discontinuity tracked by the moving mesh is indicated by the dashed line.

(b) Density at $t = 0.7$, moving mesh, $N = 100$.(c) Velocity u at $t = 0.7$, uniform grid, $N = 2000$.



(d) Velocity u at $t = 0.7$, moving mesh, $N = 100$.



(e) Pressure p at $t = 0.7$, uniform grid, $N = 100$.

Figure 5. (cont.)

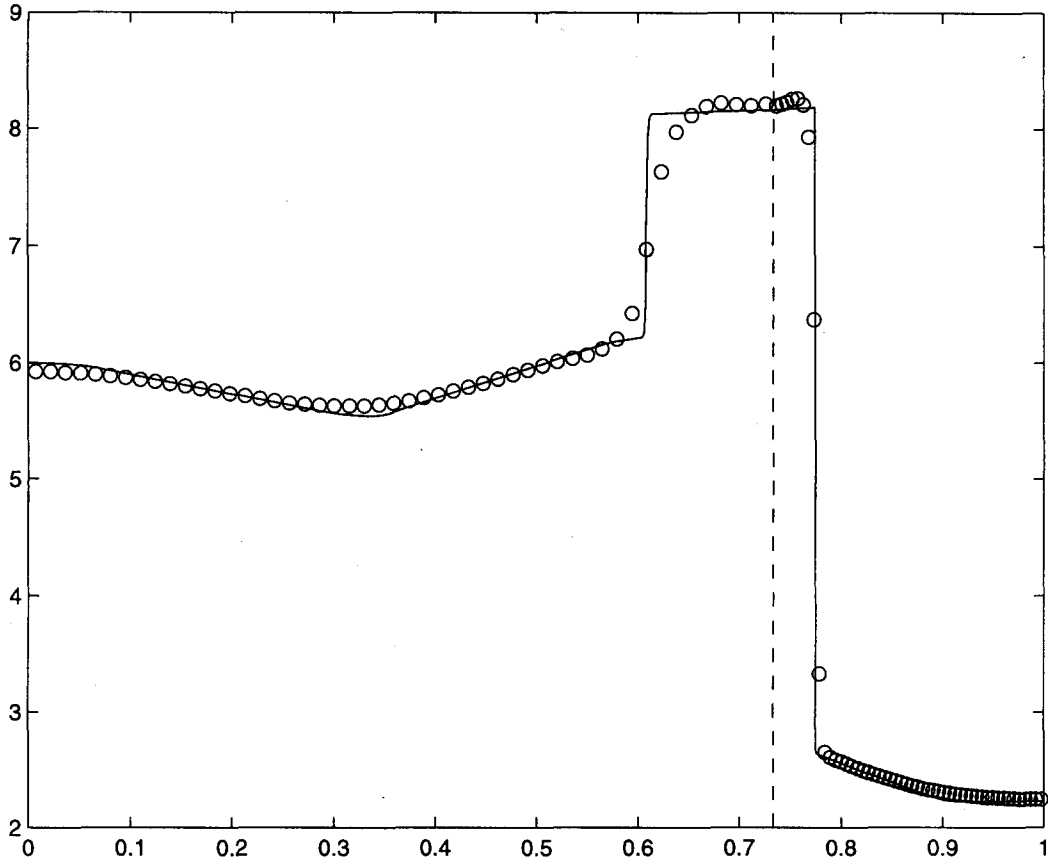
(f) Pressure p at $t = 0.7$, moving mesh, $N = 100$.

Figure 5. (cont.)

CASE 1.

$$\mathbf{q}_1 = (\rho_1, u_1, p_1) = \begin{cases} (4.3333, 3.2817, 15.0), & \text{postshock, air, } 0 \leq x < 0.3, \\ (1.0, 0.0, 1.0), & \text{preshock, air, } 0.3 < x < 0.5, \end{cases}$$

$$\mathbf{q}_2 = (\rho_2, u_2, p_2) = (0.1379, 0.0, 1.0), \quad \text{preshock, helium, } 0.5 < x \leq 1,$$

with $\gamma_1 = 1.4$ and $\gamma_2 = 1.67$.

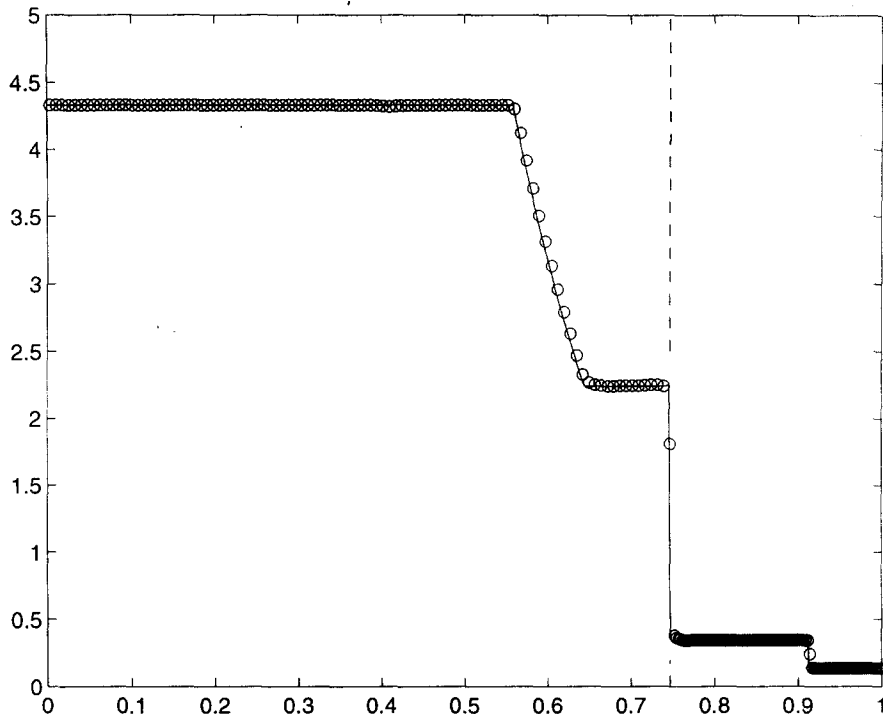
CASE 2. The data for \mathbf{q}_1 to the left of the interface is as given in the previous test. To the right of the interface is the heavier gas R22,

$$\mathbf{q}_2 = (\rho_2, u_2, p_2) = (3.1538, 0.0, 1.0), \quad \text{preshock, R22, } 0.5 < x \leq 1,$$

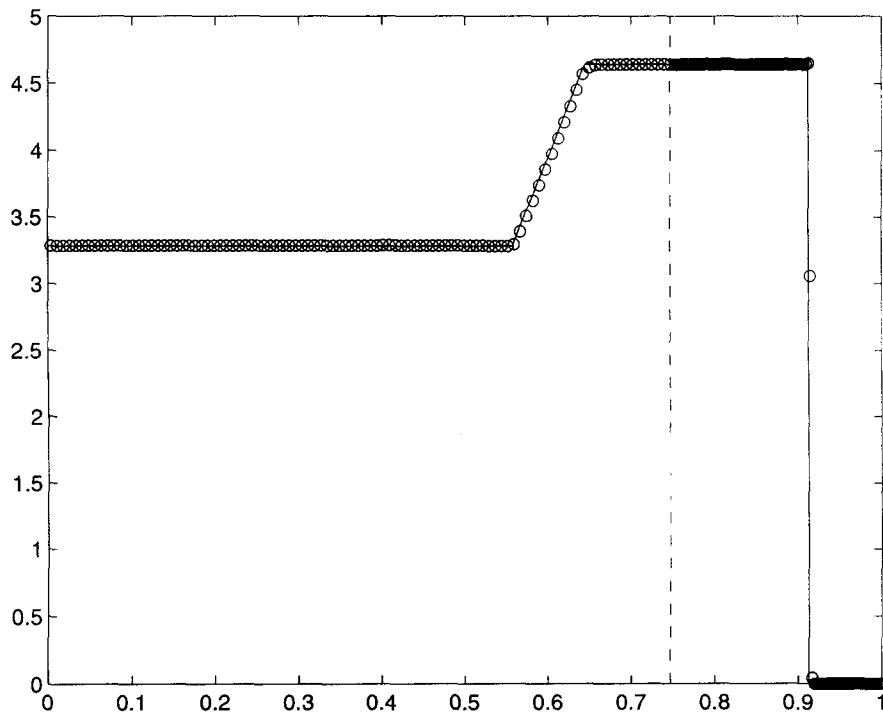
with $\gamma_1 = 1.4$ and $\gamma_2 = 1.249$.

In both cases, we apply inflow (outflow) boundary conditions at the left (right) boundary.

Figure 6 illustrates the field variables at a time after the shock-interface interaction for the two cases of this example.

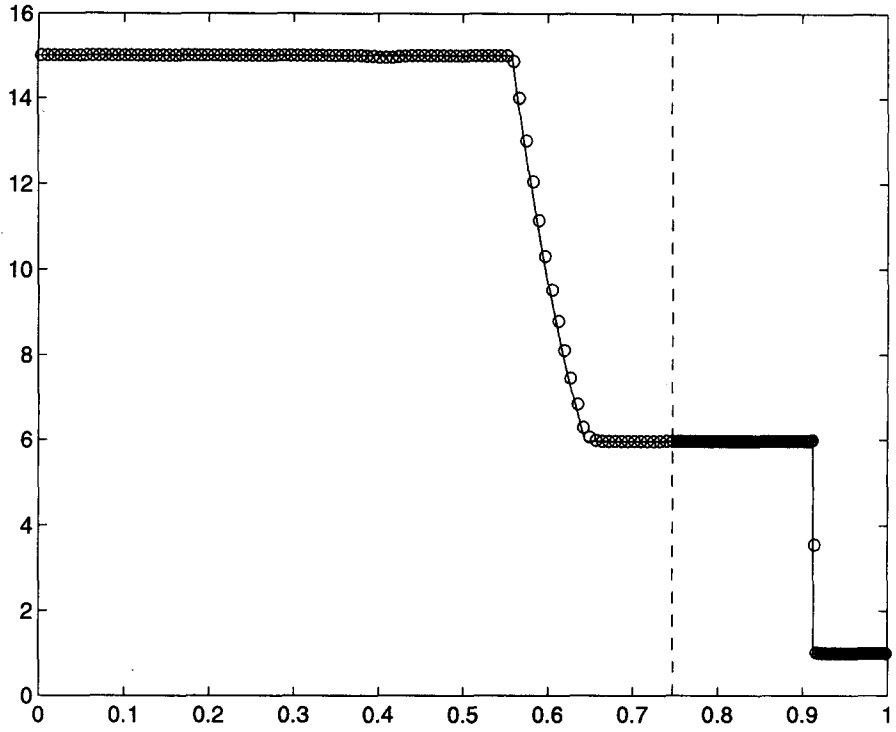


(a) Case 1: density.

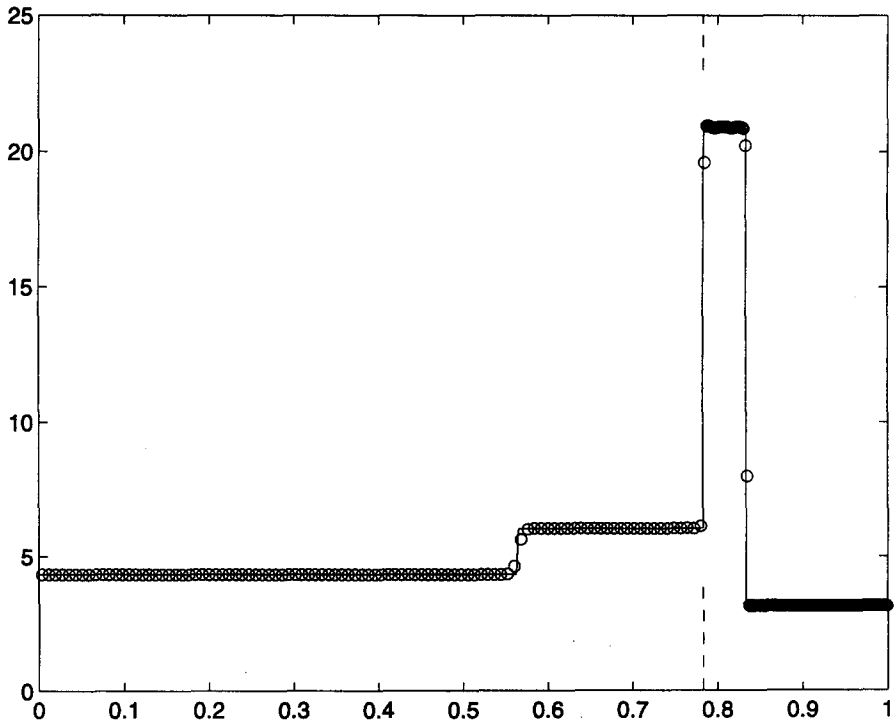


(b) Case 1: velocity.

Figure 6. Numerical results for Example 2. The circles and solid line are computed using 200 and 2000 mesh-cells, respectively. The position of the computed interface is marked by a dashed line.

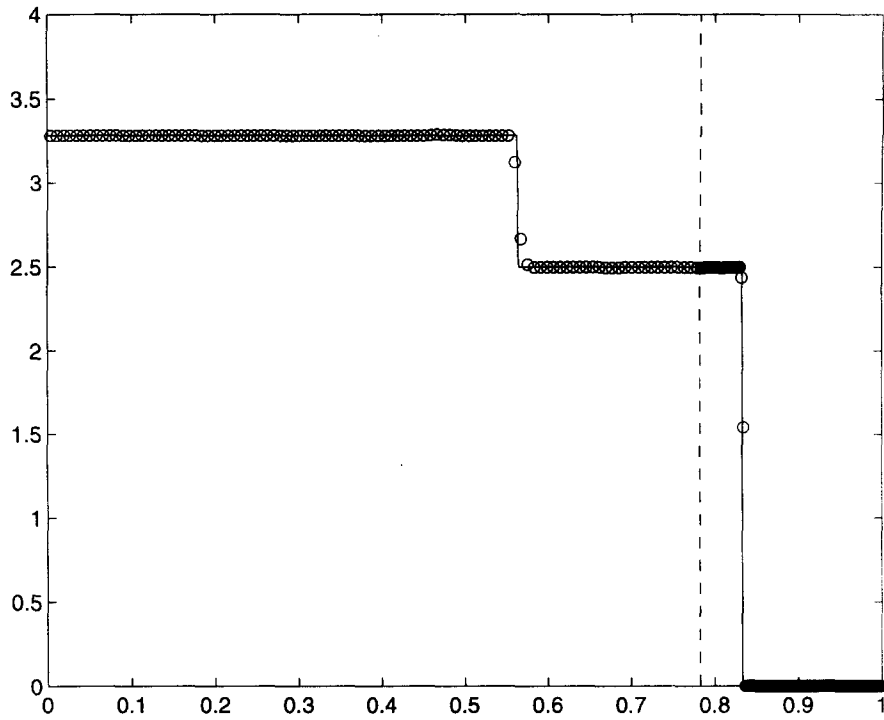


(c) Case 1: pressure.

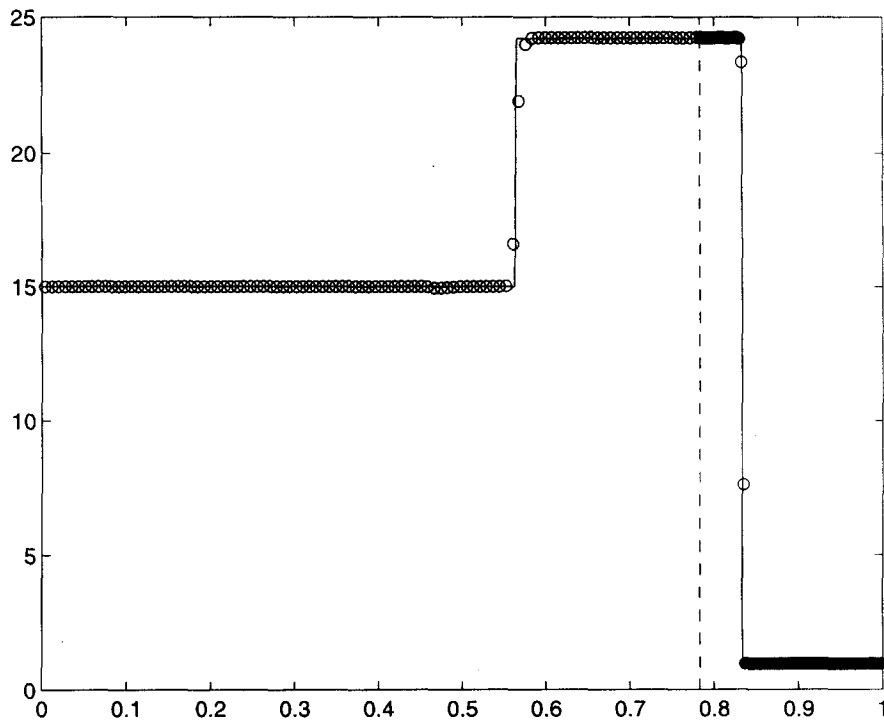


(d) Case 2: density.

Figure 6. (cont.)



(e) Case 2: velocity.



(f) Case 2: pressure.

Figure 6. (cont.)

Note that, for both tests, the entire flow field is supersonic and that the transmitted waves are shocks. On the other hand, the reflected wave is a rarefaction in the first test and a shock in the second one. Note also how our scheme accurately locates all wave positions; this can be compared with the results obtained by the hybrid algorithm of [14] and contrasted with the results given by the ghost fluid method of [16].

EXAMPLE 3.

Next we consider a more interesting problem where there are two different gases in the tube, with $\gamma = 1.4$ for $x < 0.5$ and $\gamma = 2.8$ for $x > 0.5$. In addition, the right end of the tube is now a piston at position $x = L(t)$, which is free to move without friction in the tube. The piston separates the gas under study from the exterior environment which is assumed to be held at constant pressure p_{out} . The piston has a mass m , surface area A , and is accelerated by the pressure difference $p(L(t), t) - p_0$ between the interior and exterior gas at the piston. In each time step, the pressure in the final grid cell is used to calculate this acceleration $\ddot{L}(t_n)$, according to

$$\ddot{L}(t_n) = \frac{A}{m} (p_N^n - p_{\text{out}}),$$

where p_N^n is the pressure in the rightmost grid cell at time t_n . This is used to update the piston velocity \dot{L}^n and position L^n by

$$\begin{aligned}\dot{L}^n &= \dot{L}^{n-1} + \Delta t \ddot{L}(t_n), \\ L^{n+1} &= L^n + \Delta t \dot{L}^n.\end{aligned}$$

Initially the piston is stationary: $L^0 = 1$ and $\dot{L}^0 = 0$. The solid wall boundary condition at the piston is imposed by setting values in two ghost cells $i = N + 1$ and $i = N + 2$ following the general approach of [1], with

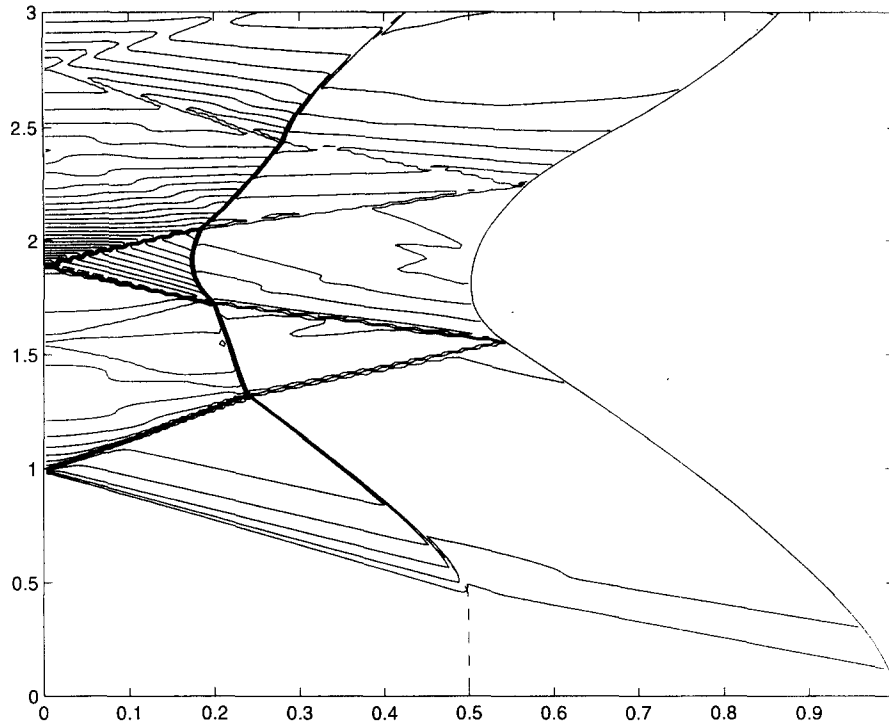
$$\begin{aligned}\rho_{N+1} &= \rho_N, & \rho_{N+2} &= \rho_{N+1}, \\ u_{N+1} &= 2\dot{L}^n - u_N, & u_{N+2} &= 2\dot{L}^n - u_{N+1}, \\ p_{N+1} &= p_N, & p_{N+2} &= p_{N+1}.\end{aligned}$$

This is simply a reflection of the data at the boundary with the velocity reflected in such a way that the piston moves along the contact discontinuity in the resulting solution to the Riemann problem at the right boundary.

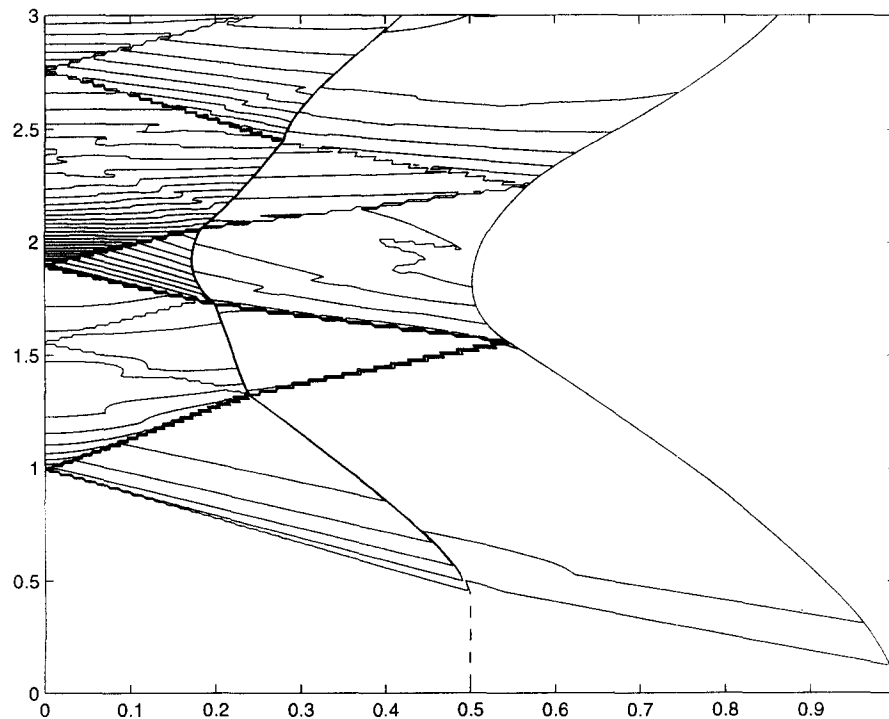
In the calculations presented here, $A/m = 2$ was used. Initially, the gas in the tube is taken to have uniform density, pressure, and zero velocity, with $\rho \equiv 1$, $p \equiv 0.5$, while $p_{\text{out}} = 1$. The pressure difference $p - p_{\text{out}}$ causes the piston to smoothly accelerate inwards, leading to a compression wave which is amplified as it passes through the interface at $x = 0.5$ into the more compressible gas with smaller γ .

Figure 7 shows contours of density for calculations with 100 and 2000 grid cells, over the time interval $0 \leq t \leq 3$. Figure 8 shows the computed density and pressure at $t = 3.0$ for grids with 100 and 200 cells, in each case compared to the 2000-cell reference solution.

Figure 9 shows $I(t)$ and $L(t)$ for 100-cell and 2000-cell calculations taken out to much larger time, $0 \leq t \leq 20$. The coarse grid calculation gives nearly the same behavior as the fine grid reference solution. Only for large t is any difference visible to plotting accuracy, and even then the qualitative structure is very close.

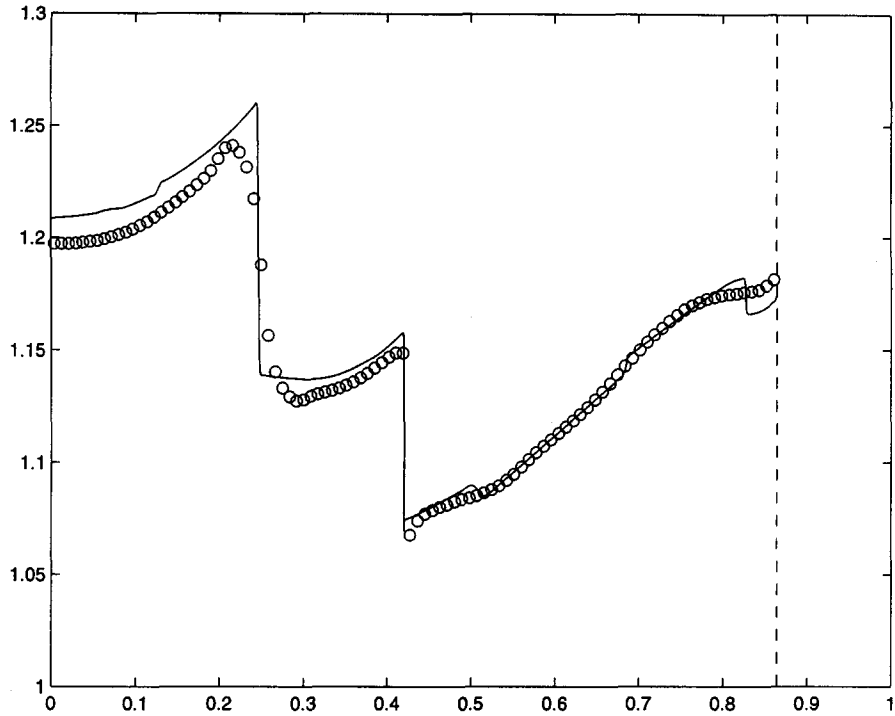


(a) Density contours in $x-t$ plane. (100 mesh cells.)

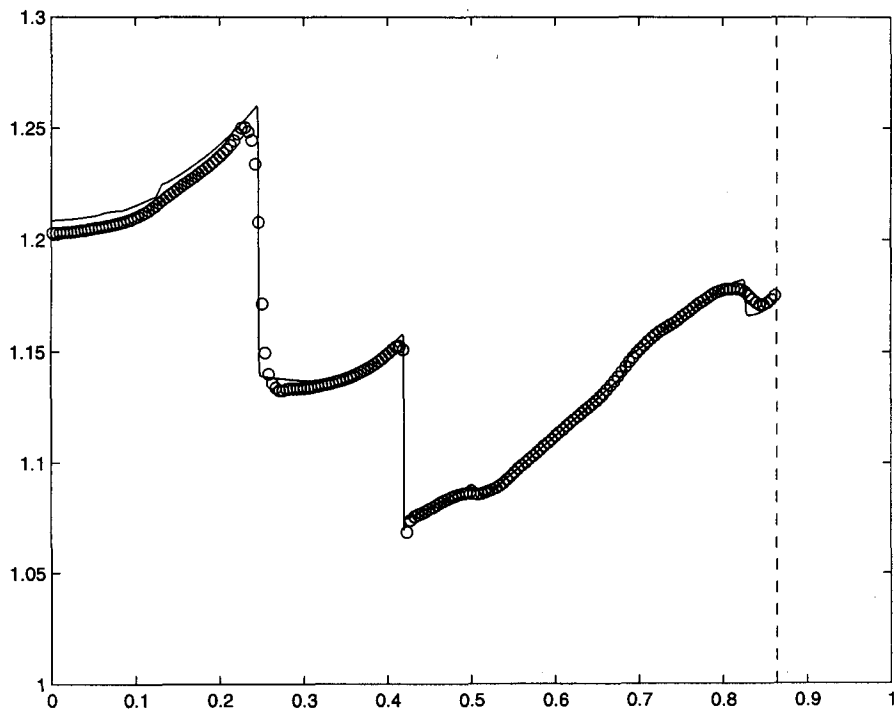


(b) Density contours in $x-t$ plane. (2000 mesh cells.)

Figure 7. (a). Motion of the interface $I(t)$ and the piston $L(t)$ for Example 3. Contour plots of density in the $x-t$ plane for Example 3, two different computations with the moving-mesh tracking both the interface motion $I(t)$ and the piston motion $L(t)$.

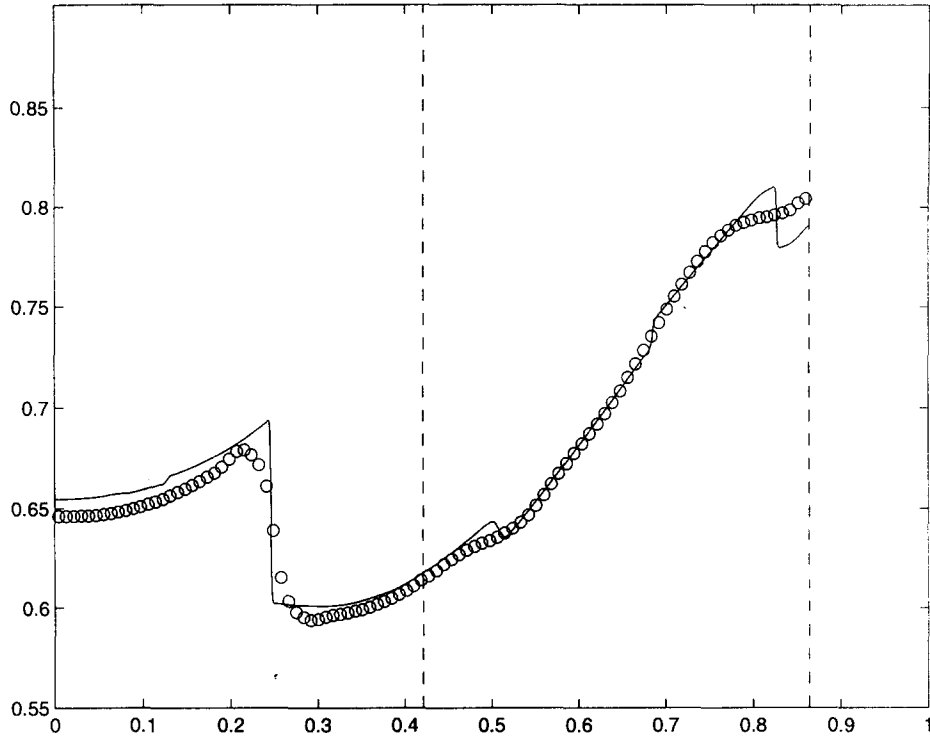


(a) Rho (density) for the 100-cell moving mesh.

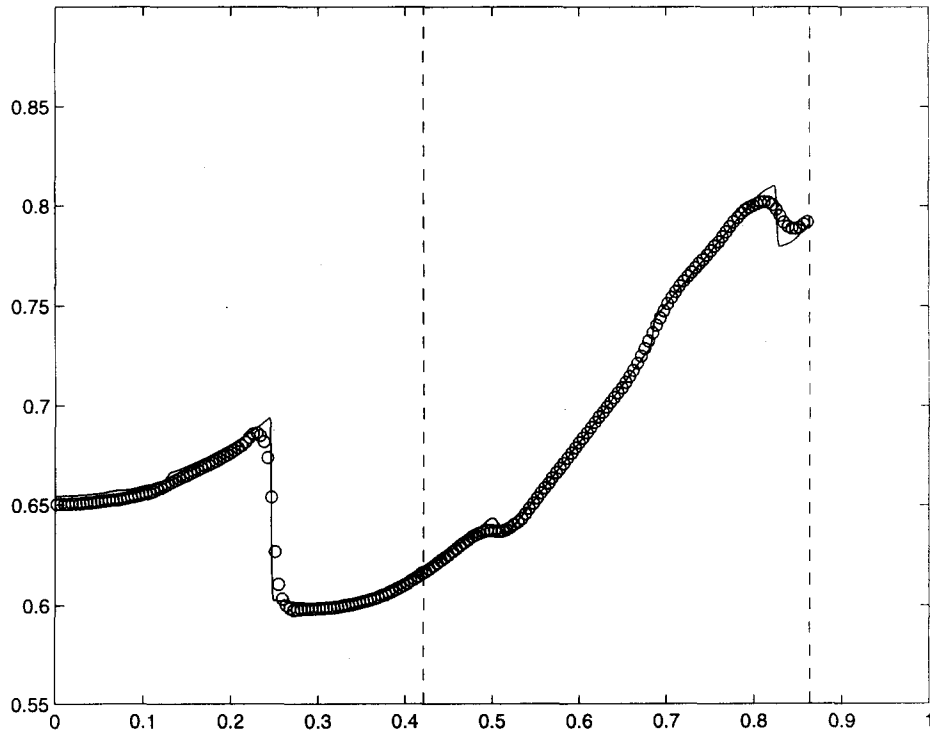


(b) Rho (density) for the 200-cell moving mesh.

Figure 8. The computed solution to Example 3 at one particular time $t = 3.0$ for the 100-cell moving mesh and the 200-cell moving mesh. In each case, the solid line reference solution is from the 2000-cell moving-mesh calculation. The contact discontinuity $I(t)$ and the piston location $L(t)$ at this time are indicated by the dashed line.

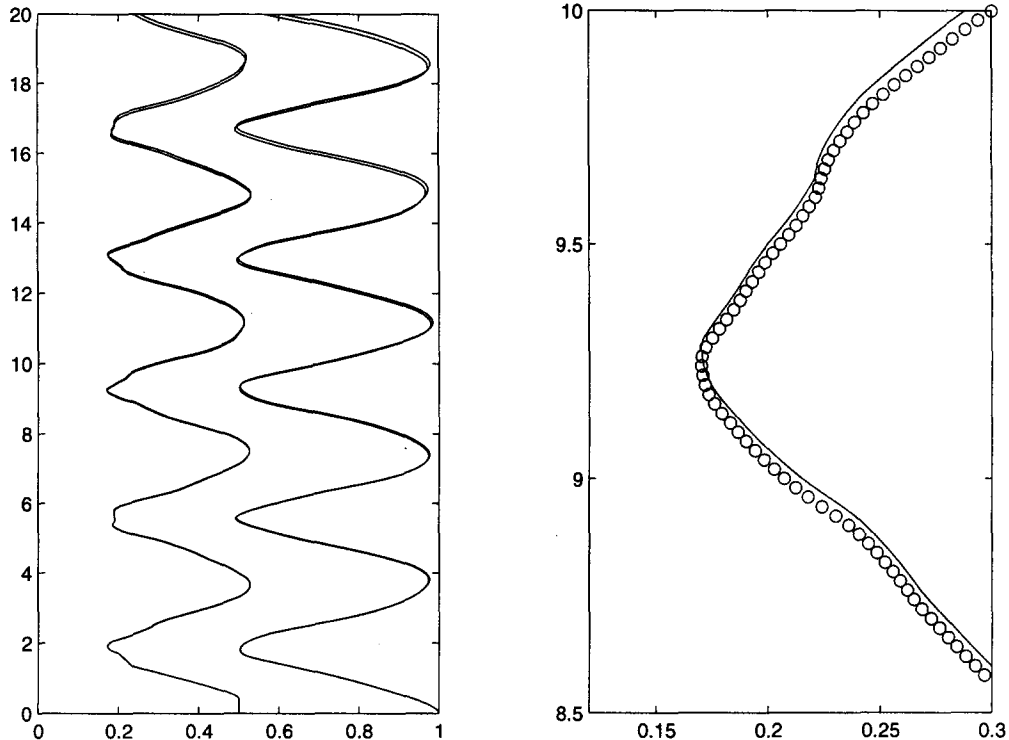


(c) Pressure for the 100-cell moving mesh.



(d) Pressure for the 200-cell moving mesh.

Figure 8. (cont.)



(a) Motion of the interface $I(t)$ and the piston $L(t)$ for Example 3. Curves from two different computations with 100 cells and 2000 cells are plotted together.

(b) Blow-up of this plot near one reversal of $I(t)$. In this plot, the solid line is the 2000-cell result and the symbols indicate $I(t)$ for the 100-cell result.

Figure 9.

7. CONCLUSIONS AND EXTENSIONS

We have developed a general one-dimensional moving-mesh method for hyperbolic systems of conservation laws. The test problems presented here demonstrate that this algorithm can be used to obtain high resolution results in problems where a fluid interface or moving boundary interacts both with strong shock waves and with smooth flow.

We have chosen a simple strategy for distributing the mesh points, equally spaced within each gas, to illustrate the algorithm for multifluid problems. The results indicate that good accuracy is obtained even when there is a large jump in the cell size at the interface, a robustness feature which is important more generally. It would be quite easy to couple this method with other procedures for moving the mesh points. For example, Stockie, Mackenzie and Russell [17] recently coupled our method together with an additional equation for redistribution of the mesh points based on error estimation. They have applied the method to cluster grid points near shock waves in Burgers', Euler, and Buckley-Leverett equations.

In one space dimension, it is generally possible to compute on a very fine grid and so the need for moving-mesh methods may not be so clear. However, the use of our method requires very little additional computation and can provide significantly better resolution on any particular grid. It is based on the wave-propagation algorithm and CLAWPACK software, which can easily be adapted to other hyperbolic problems. Moreover, there are problems where a moving grid is preferable to a fixed grid for physical reasons. For example, the moving piston problem of Example 3 cannot be solved on a fixed grid, unless this is combined with some form of front tracking or another approach to handle the changing domain. Examples 2 and 3 also involve a physical interface between different gases. On a fixed grid, this interface would move relative to

the grid, resulting in cells containing a mixture of the gases. Resolving the solution accurately near the interface then requires special methods, as studied in [14], for example. The moving-mesh method keeps the two gases distinct. This approach can be easily generalized to handle problems with more interfaces. In fact, it is possible to use this approach to study the propagation of waves through a rapidly varying or random material (as in [5,6]) in the fully nonlinear case. There are interesting homogenization questions that are still not well understood in the one-dimensional case. We hope that the moving-mesh method, by providing an accurate solution of the true problem, may aid in the investigation of these propagation phenomena and the study of homogenization procedures. This is currently being investigated.

A natural question is whether this approach can be extended to more than one dimension. Multidimensional moving-mesh methods are often difficult to use in fluid dynamics problems since the grid will typically suffer large distortions and possible tangling. However, for hyperbolic wave propagation problems in heterogeneous solids, it would be very useful to have a moving-mesh method that follows relatively small deformations of the material. This would allow the interfaces between different materials to remain well defined, and allow the solution of appropriate Riemann problems at these interfaces to correctly model the transmission and reflection of waves.

Multidimensional versions of the wave propagation algorithm are presented in [1,18] and implemented in the CLAWPACK software. These methods are again based on solving one-dimensional Riemann problems, and apply to a wide variety of hyperbolic systems. The principal difficulty in extending the moving-mesh method to multidimensions is the fact that a space-time interface between cells is no longer a surface along which the Riemann solution is constant, except in certain special cases, and hence, the numerical flux through this surface is harder to define. However, it can be chosen as a ruled surface defined by the movement of the corners, and this appears to allow the development of good approximate fluxes. This extension is currently being developed and will be reported elsewhere.

REFERENCES

1. R.J. LeVeque, Wave propagation algorithms for multi-dimensional hyperbolic systems, *J. Comput. Phys.* **131**, 327–353, (1997).
2. R.J. LeVeque, *CLAWPACK software*, <http://www.amath.washington.edu/~rjl/clawpack.html>.
3. A. Harten and J.M. Hyman, Self-adjusting grid methods for one-dimensional hyperbolic conservation laws, *J. Comput. Phys.* **50**, 235–269, (1983).
4. C.C. Wu and P.H. Roberts, Shock-waves propagation in a sonoluminescing gas bubble, *Phys. Rev. Lett.* **70**, 3424–3427, (1993).
5. T. Fogarty and R.J. LeVeque, High-resolution finite volume methods for acoustics in periodic or random media, *J. Acoust. Soc. Am.* **106**, 17–28, (1999).
6. J. Kevorkian and D.L. Bosley, Multiple-scale homogenization for weakly nonlinear conservation laws with rapid spatial fluctuations, *Stud. Appl. Math.* **101**, 127–183, (1998).
7. E.A. Dorfi and L.O'C. Drury, Simple adaptive grids for 1-D initial value problems, *J. Comput. Phys.* **69**, 175, (1987).
8. W.Z. Huang, Y. Ren and R.D. Russell, Moving mesh methods based on moving mesh partial differential equations, *J. Comput. Phys.* **113**, 279, (1994).
9. S. Li and L. Petzold, Moving mesh methods with upwinding schemes for time-dependent PDEs, *J. Comput. Phys.* **131**, 368–377, (1997).
10. N.N. Carlson and K. Miller, Design and application of gradient-weighted moving finite element code. I: In one dimension, *SIAM J. Sci. Comput.* **19**, 728–765, (1998).
11. Y. Ren and R.D. Russell, Moving mesh techniques based upon equidistribution, and their stability, *SIAM J. Sci. Comput.* **13**, 1265–1286, (1992).
12. K. Saleri and S. Steinberg, Flux-corrected transport in a moving grid, *J. Comput. Phys.* **111**, 24, (1994).
13. R. Fazio and D.J. Evans, An implicit difference scheme for a moving boundary hyperbolic problem, *Appl. Numer. Math.* **12**, 485–496, (1993).
14. S. Karni, Hybrid multifluid algorithms, *SIAM J. Sci. Comput.* **17**, 1019–1039, (1996).
15. P. Jenny, B. Müller and H. Thomann, Correction of conservative Euler solvers for gas mixture, *J. Comput. Phys.* **132**, 91–107, (1997).
16. R.P. Fedkiw, T. Aslam, B. Merriman and S. Osher, A non-oscillatory Eulerian approach to interfaces in multimaterial flows (the ghost fluid method), *J. Comput. Phys.* **152**, 457–492, (1999).

17. J.M. Stockie, J.A. Mackenzie and R.D. Russell, A moving mesh method for one-dimensional hyperbolic conservation laws, *SIAM J. Sci Comput.* **22**, 1791–1813, (2001); <http://www.math.sfu.ca/~jms/papers/hyp-abstract.html>.
18. J.O. Langseth and R.J. LeVeque, A wave-propagation method for three-dimensional hyperbolic conservation laws, *J. Comput. Phys.* **165**, 126–166, (2000); <ftp://amath.washington.edu/pub/rjl/papers/jol-rjl:3d.ps.gz>, (1999).